J|A|C|S ARTICLES

Published on Web 09/02/2009

The Pyrrolobenzodiazepine Dimer SJG-136 Forms Sequence-Dependent Intrastrand DNA Cross-Links and Monoalkylated Adducts in Addition to Interstrand Cross-Links

Khondaker M. Rahman,[†] Andrew S. Thompson,[‡] Colin H. James,[†] Mathangi Narayanaswamy,[†,§] and David E. Thurston*[,†,§]

Gene Targeted Drug Design Research Group, The School of Pharmacy, University of London, 29/39 Brunswick Square, London WC1N 1AX, U.K., Department of Pharmacy and Pharmacology, University of Bath, Bath BA2 7AY, U.K., and Spirogen Ltd., The School of Pharmacy, University of London WC1N 1AX, U.K.

Received April 23, 2009; E-mail: david.thurston@pharmacy.ac.uk

Abstract: SJG-136 (**1**) is a sequence-selective DNA-interactive agent that is about to enter phase II clinical trials. Using a HPLC/MS-based methodology developed to evaluate the binding of DNA-interactive agents to oligonucleotides of varying length and sequence, we have demonstrated that, in addition to the previously known interstrand cross-link at Pu-GATC-Py sequences, **1** can form a longer interstrand cross-link at Pu-GAATC-Py sequences, an intrastrand cross-link at both shorter Pu-GATG-Py and longer Pu-GAATG-Py sequences, and, in addition, monoalkylated adducts at suitable PBD binding sites where neither intra- or interstrand cross-links are feasible because of the unavailability of two appropriately positioned guanines. Crucially, we have demonstrated a preference for the extended intrastrand cross-link with Pu-GAATG-Py, which forms more rapidly than the other cross-links (rank order: Pu-GAATG-Py > Pu-GATC-Py ≫ Pu-GATG-Py and Pu-GAATC-Py). However, thermal denaturation studies suggest that the originally reported Pu-GATC-Py interstrand cross-link is more stable, consistent with the covalent joining of both strands of the duplex and a lower overall distortion of the helix according to modeling studies. These observations impact on the proposed mechanism of action of SJG-136 (**1**) both in vitro and in vivo, the repair of its adducts and mechanism of resistance in cells, and potentially on the type of pharmacodynamic assay used in clinical trials.

Introduction

The majority of clinically employed bifunctional alkylating agents form interstrand and/or intrastrand DNA cross-links that cause arrest of the replication fork.[1] In addition to this effect on replication, such agents can also prevent the DNA binding of control and processing proteins critical for transcription.[2,3] DNA cross-linking agents, whether intra- or interstrand adduct-forming (or both), can be highly toxic to healthy cells as well as tumor cells, thus leading to their well-known side effects.[4] The most likely basis for selectivity appears to be preferential DNA repair in healthy cells, with the repair response to different cross-linking agents in tumor cells varying, depending on cell type and the extent and duration of exposure to a particular agent.[5] The ability of tumor cells to carry out DNA repair will, along with other factors, influence the development of resistance which can affect both in vitro and in vivo efficacy.

Pyrrolo[2,1-*c*][1,4]benzodiazepine (PBD) dimers are synthetic sequence-selective DNA minor-groove cross-linking agents developed from the tricyclic anthramycin family of naturally occurring antitumor antibiotics (Figure 1A).[6−9] PBDs have a chiral C11a(*S*)-position which provides them with an appropriate shape to fit securely in the minor groove of DNA.[8] In addition, they possess an electrophilic N10−C11 moiety (i.e., interconvertible imine, carbinolamine, or carbinolamine methyl ether functionalities) that can form a covalent aminal linkage between their C11-position and the nucleophilic C2-NH_2 group of a guanine base (Figure 1B).[8] PBD monomers (e.g., anthramycin and tomaymycin; Figure 1A) typically span three base pairs of DNA with a preference for 5′-Pu-G-Pu-3′ sequences.[8] However, the synthetic PBD dimers such as SJG-136 (**1**) and DSB-120 (**2**) (Figure 1A) can span six or more base pairs, depending on the length of the C8/C8′-linker connecting the monomeric

[†] Gene Targeted Drug Design Research Group, University of London.
[‡] University of Bath.
[§] Spirogen Ltd., University of London.

(1) Bae, J. B.; Mukhopadhyay, S. S.; Liu, L.; Zhang, N.; Tan, J.; Akhter, S.; Liu, X.; Shen, X.; Li, L.; Legerski, R. J. *Oncogene* **2008**, *27*, 5045–5056.
(2) Gray, P. J. *Nucleic Acids Res.* **1995**, *23*, 4378–4382.
(3) Dhar, S.; Lippard, S. J. *Platinum and Other Heavy Metal Compounds in Cancer Chemotherapy*; Humana Press: Totowa, NJ, 2009; p 135147.
(4) Thurston, D. E. *Chemistry and Pharmacology of Anticancer Drugs*; CRC Press (Taylor & Francis): Boca Raton, FL, 2006; pp 281.
(5) Andreassen, P. R.; Ren, K. Q. *Curr. Cancer Drug Targets* **2009**, *9*, 101–117.
(6) Cipolla, L.; Araujo, A. C.; Airoldi, C.; Bini, D. *Anti-Cancer Agents Med. Chem.* **2009**, *9*, 1–31.
(7) Thurston, D. E.; Bose, D. S. *Chem. Rev.* **1994**, *94*, 433–465.
(8) Thurston, D. E. In *Molecular Aspects of Anticancer Drug-DNA Interactions*; Neidle, S., Waring, M. J. , Eds.; The Macmillan Press Ltd.: London, U.K., 1993; Vol. 1, pp 54−88.
(9) Kamal, A.; Rao, M. V.; Laxman, N.; Ramesh, G.; Reddy, G. S. K. *Curr. Med. Chem.: Anti-Cancer Agents* **2002**, *2*, 215–254.

 10.1021/ja902986x CCC: $40.75

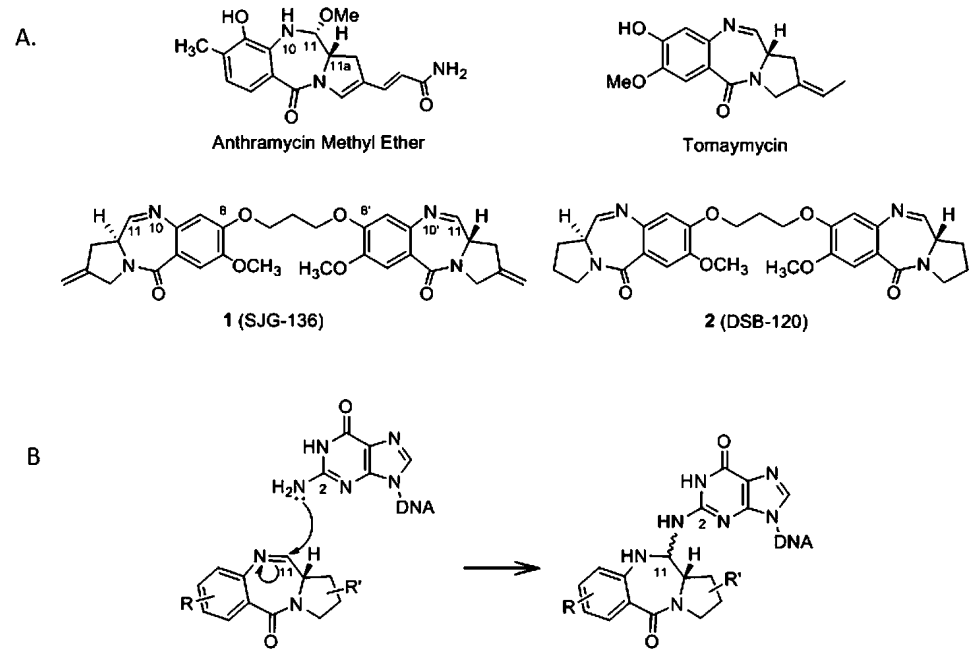

Figure 1. (A) Structures of the naturally occurring monoalkylating pyrrolobenzodiazepine (PBD) monomers, anthramycin and tomaymycin, and the synthetic PBD dimers SJG-136 (**1**) and DSB-120 (**2**). (B) Schematic diagram of a monomeric PBD binding covalently through its C11-position to the C2-NH_2 of a guanine base within the minor groove of DNA.

units.[6,10] PBD monomers and dimers have been shown to mediate a number of biological effects including the inhibition of endonucleases,[11] RNA polymerase,[12,13] and transcription factor DNA binding.[14]

The structure of PBD adducts has been studied by high-field NMR,[15,16] molecular modeling,[10,16−18] mass spectrometry,[19] and biochemical methods.[20] To date, the biological activity of PBD dimers has been thought to reside mainly in their ability to form sequence-selective interstrand guanine−guanine cross-links, and this adduct formed by SJG-136 (**1**) has been used as a pharmacodynamic endpoint during phase I clinical trials.[21] The molecule is known to form interstrand cross-links at Pu-GATC-Py sequences, laying snugly in the minor groove with its two PBD units forming covalent bonds to the C2-NH_2 groups of guanines on either strand. Through this arrangement, the molecule spans a total of six base pairs while specifically recognizing the central GATC palindrome (Figure 2A and 2C).[22] This binding preference has been rationalized based on NMR and molecular modeling studies of the C2-unsubstituted parent molecule DSB-120 (**2**)[23,24] and through COMET and gel electrophoresis (i.e., agarose gel cross-linking[25] and footprinting[20]) studies on SJG-136. In particular, hydrogen bonds between the N10 protons of the two PBD units and the adjacent central adenines on either strand are thought to give rise to the selectivity for the inner A.T/T.A base pairs.[22]

Until now, this interstrand cross-link was assumed to be the only type of adduct formed by SJG-136. However, some recent high-field NMR data (Thompson, A.S., unpublished results) suggested that intrastrand cross-links may also form at Pu-GATG-Py sequences. We have investigated this using a HPLC/MS-based assay[19] developed in our laboratory for studying the interaction of DNA-binding agents with oligonucleotides of varying length and sequence. Through these studies we have been able to establish that, in addition to the previously reported interstrand cross-links at Pu-GATC-Py sequences, **1** can form intrastrand cross-links at Pu-GATG-Py and Pu-GAATG-Py (Figure 2B and 2D) motifs with a preference for the latter. In

(10) Gregson, S. J.; Howard, P. W.; Gullick, D. R.; Hamaguchi, A.; Corcoran, K. E.; Brooks, N. A.; Hartley, J. A.; Jenkins, T. C.; Patel, S.; Guille, M. J.; Thurston, D. E. *J. Med. Chem.* **2004**, *47*, 1161–1174.
(11) Puvvada, M. S.; Hartley, J. A.; Jenkins, T. C.; Thurston, D. E. *Nucleic Acids Res.* **1993**, *21*, 3671–3675.
(12) Wells, G.; Martin, C. R. H.; Howard, P. W.; Sands, Z. A.; Laughton, C. A.; Tiberghien, A.; Woo, C. K.; Masterson, L. A.; Stephenson, M. J.; Hartley, J. A.; Jenkins, T. C.; Shnyder, S. D.; Loadman, P. M.; Waring, M. J.; Thurston, D. E. *J. Med. Chem.* **2006**, *49*, 5442–5461.
(13) Puvvada, M. S.; Forrow, S. A.; Hartley, J. A.; Stephenson, P.; Gibson, I.; Jenkins, T. C.; Thurston, D. E. *Biochemistry* **1997**, *36*, 2478–2484.
(14) Kotecha, M.; Kluza, J.; Wells, G.; O'Hare, C. C.; Forni, C.; Mantovani, R.; Howard, P. W.; Morris, P.; Thurston, D. E.; Hartley, J. A.; Hochhauser, D. *Mol. Cancer Ther.* **2008**, *7*, 1319–1328.
(15) Antonow, D.; Barata, T.; Jenkins, T. C.; Parkinson, G. N.; Howard, P. W.; Thurston, D. E.; Zloh, M. *Biochemistry* **2008**, *47*, 11818–11829.
(16) Jenkins, T. C.; Hurley, L. H.; Neidle, S.; Thurston, D. E. *J. Med. Chem.* **1994**, *37*, 4529–4537.
(17) Reddy, B. S. P.; Sharma, S. K.; Lown, J. W. *Curr. Med. Chem.* **2001**, *8*, 475–508.
(18) Smellie, M.; Bose, D. S.; Thompson, A. S.; Jenkins, T. C.; Hartley, J. A.; Thurston, D. E. *Biochemistry* **2003**, *42*, 8232–8239.
(19) Narayanaswamy, M.; Griffiths, W. J.; Howard, P. W.; Thurston, D. E. *Anal. Biochem.* **2008**, *374*, 173–181.
(20) Martin, C.; Ellis, T.; McGurk, C. J.; Jenkins, T. C.; Hartley, J. A.; Waring, M. J.; Thurston, D. E. *Biochemistry* **2005**, *44*, 4135–4147.
(21) Hochhauser, D.; Meyer, T.; Spanswick, V. J.; Wu, J.; Clingen, P. H.; Loadman, P. M.; Cobb, M.; Gumbrell, L.; Begent, R. H. J.; Hartley, J. A.; Jodrell, D. I. *Clin. Cancer Res.* **2009**, *15*, 2140–2147.
(22) Gregson, S. J.; Howard, P. W.; Hartley, J. A.; Brooks, N. A.; Adams, L. J.; Jenkins, T. C.; Kelland, L. R.; Thurston, D. E. *J. Med. Chem.* **2001**, *44*, 737–748.
(23) Bose, D. S.; Thompson, A. S.; Ching, J. S.; Hartley, J. A.; Berardini, M. D.; Jenkins, T. C.; Neidle, S.; Hurley, L. H.; Thurston, D. E. *J. Am. Chem. Soc.* **1992**, *114*, 4939–4941.
(24) Mountzouris, J. A.; Wang, J. J.; Thurston, D.; Hurley, L. H. *J. Med. Chem.* **1994**, *37*, 3132–3140.
(25) Hartley, J. A.; Spanswick, V. J.; Brooks, N.; Clingen, P. H.; McHugh, P. J.; Hochhauser, D.; Pedley, R. B.; Kelland, L. R.; Alley, M. C.; Schultz, R.; Hollingshead, M. G.; Schweikart, K. M.; Tomaszewski, J. E.; Sausville, E. A.; Gregson, S. J.; Howard, P. W.; Thurston, D. E. *Cancer Res.* **2004**, *64*, 6693–6699.

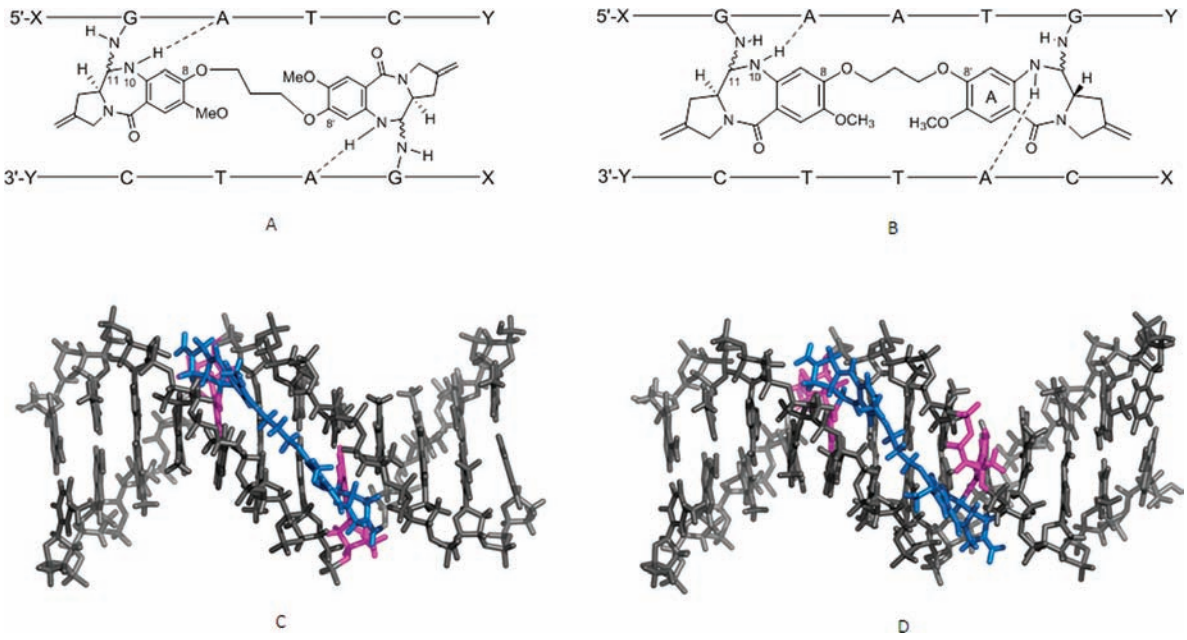

Figure 2. (A and C) Schematic diagram and molecular model, respectively, of the *interstrand* cross-linked adduct formed by interaction of SJG-136 (**1**) with Pu-GATC-Py. (B and D) Schematic diagram and molecular model, respectively, of the *intrastrand* adduct formed by interaction of **1** with Pu-GAATG-Py. Note: In models C and D, the DNA, SJG-136 (**1**) and the guanines to which **1** is covalently bound are colored gray, blue and magenta, respectively. In Diagram B, as the right-hand PBD unit is oriented with A-ring 5′ (relative to the bonded strand), the N10′-proton can form a hydrogen bond to the nearby adenine on the opposite strand.

Table 1. Structures of the Single-Stranded (SS) Oligonucleotides Used in the Study and the Duplexes Formed from Them[a]

label	SS DNA sequence	label	DS DNA sequence
Seq-1	5′-TATAGATCTATA-3′	Duplex-1	5′-TATAGATCTATA-3′ 3′-ATATCTAGATAT-5′
Seq-2	5′-TATAGATGTATA-3′	Duplex-2	5′-TATAGATGTATA-3′
Seq-3	5′-TATACATCTATA-3′		3′-ATATCTACATAT-5′
Seq-4	5′-TATAGAATCTATA-3′	Duplex-3	5′-TATAGAATCTATA-3′
Seq-5	5′-TATAGATTCTATA-3′		3′-ATATCTTAGATAT-5′
Seq-6	5′-TATAGAATGTATA-3′	Duplex-4	5′-TATAGAATGTATA-3′
Seq-7	5′-TATACATTCTATA-3′		3′-ATATCTTACATAT-5′
Seq-2A_{ino}	5′-TATAGATITATA-3′	Duplex-2A_{ino}	5′-TATAGATITATA-3′ 3′-ATATCTACATAT-5′
Seq-2B_{ino}	5′-TATAIATGTATA-3′	Duplex-2B_{ino}	5′-TATAIATGTATA-3′ 3′-ATATCTACATAT-5′
Seq-8	5′-TATAGCTATA-3′	Duplex-5	5′-TATAGCTATA-3′ 3′-ATATCGATAT-5′
Seq-9	5′-TATAGGTATA-3′	Duplex-6	5′-TATAGGTATA-3′
Seq-10	5′-TATACCTATA-3′		3′-ATATCCATAT-5′
Seq-11	5′-TATAGAAAATGTATA-3′	Duplex-7	5′-TATAGAAAATGTATA-3′
Seq-12	5′-TATACATTTTCTATA-3′		3′-ATATCTTTTACATAT-5′

[a] The numbering system for bases of individual oligonucleotides (as used in the main text) starts from the 5′-end, and potential SJG-136 binding sites are underlined.

addition, it can form monoalkylated adducts (i.e., with only one PBD unit covalently bonded) at sequences that contain suitable PBD binding sites (i.e., Pu-G-Pu) but that lack a second nearby guanine necessary for inter- or intrastrand cross-link formation.

Therefore, SJG-136 appears to form a much wider variety of adduct types than originally envisaged, which has implications for its mechanism of action, the repair of its adducts by cells, and hence their resistance to the agent. It may also influence the choice of biomarker in future clinical trials, with methods such as the gamma γH2X foci[26] assay being required to measure non-interstrand cross-linked adducts in addition to the COMET assay,[27,28] which is usually optimized to measure interstrand cross-links.

Results and Discussion

Using a modification of our previously reported HPLC/MS methodology,[19] we initially confirmed that SJG-136 (**1**) could form an interstrand cross-link at the Pu-GATC-Py sequence[22] contained within the duplex formed by the self-complementary 12-mer oligonucleotide Seq-1 (Table 1). After annealing Seq-1 (i.e., heating to 85 °C for 10 min followed by cooling to room temperature and then storing at −20 °C), HPLC analysis showed a single peak at RT 24.4 min identified as single-stranded (SS)

(26) Clingen, P. H.; Wu, J. Y. H.; Miller, J.; Mistry, N.; Chin, F.; Wynne, P.; Prise, K. M.; Hartley, J. A. *Biochem. Pharmacol.* **2008**, *76*, 19–27.
(27) Alley, M. C.; Hollingshead, M. G.; Pacula-Cox, C. M.; Waud, W. R.; Hartley, J. A.; Howard, P. W.; Gregson, S. J.; Thurston, D. E.; Sausville, E. A. *Cancer Res.* **2004**, *64*, 6700–6706.
(28) Hartley, J. M.; Spanswick, V. J.; Gander, M.; Giacomini, G.; Whelan, J.; Souhami, R. L.; Hartley, J. A. *Ann. Oncol.* **1998**, *9*, 645.

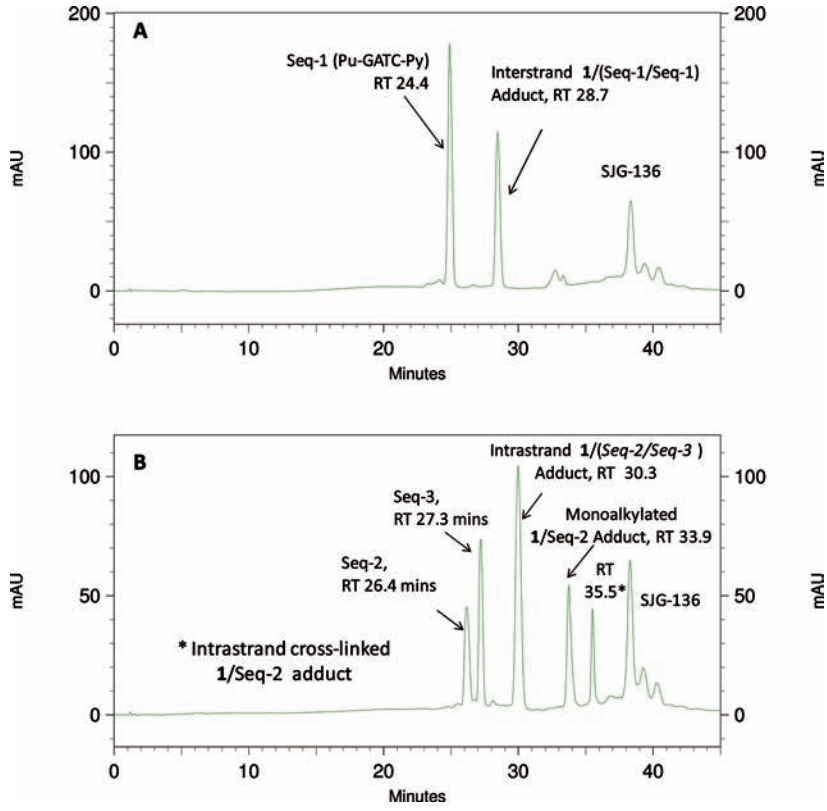

Figure 3. HPLC chromatograms: (A) Interstrand cross-linked adduct (RT 28.7 min) formed between **1** and Pu-GATC-Py (Seq-1/Seq-1 duplex) after 5 min. (B) Intrastrand cross-linked adduct (RT 30.3 min) formed between **1** and Pu-GATG-Py (Seq-2/Seq-3 duplex) after 12 h.

Seq-1 by MALDI-TOF MS. This was consistent with our previous report that DS oligonucleotides of this length denature under these HPLC conditions.[19] However, mixing the annealed duplex with **1** followed by immediate analysis (~5 min) showed the partial formation (approx 35%) of an adduct peak at RT 28.7 min (Figure 3A). A time course study showed a gradual increase in intensity of this peak until, after 3 h, it was the main product and the peak corresponding to Seq-1 had disappeared completely. On the basis of its retention time,[19] we anticipated that this product was the 1:1 **1**/(Seq-1/Seq-1) Pu-GATC-Py interstrand cross-linked adduct, and this was confirmed by MS (see Supporting Information). Excess SJG-136 (**1**) appeared as three peaks, one major (38.2 min) and two minor (39.2 and 40.2 min), assumed to represent both symmetrical and unsymmetrical N10−C11 imine and carbinolamine forms known to be present in an aqueous environment.[19]

Next, we turned to the possibility of intrastrand cross-link formation between **1** and the non-self-complementary duplex (Duplex-2) formed from oligonucleotides Seq-2/Seq-3 in which cytosine-8 of Seq-1 (5′-TATAGATCTATA-3′) was mutated to a guanine (i.e., Seq-2 = 5′-TATAGATGTATA-3′, Table 1). Analysis of the annealed duplex alone using identical HPLC conditions gave two peaks at RT 26.4 and 27.3 min, confirmed by MALDI-TOF MS to be the single-stranded Seq-2 and Seq-3, respectively. Mixing the annealed Duplex-2 with **1** showed the gradual emergence of three new peaks at RTs 30.3, 33.9, and 35.5 min (Figure 3B), the identities of which were confirmed by RT and MALDI-TOF MS (see Supporting Information). The 30.3 min peak was confirmed as the **1**/(Seq-2/Seq-3) intrastrand adduct, and a time course study showed that it remained prominent with time and accounted for 68% of the adduct peaks at the end of the experiment (i.e., 24 h). Interestingly, the ratio of peaks relating to the unreacted SS DNA species (RT = 26.4 and 27.3 min) changed in favor of the 27.3 min peak (i.e., Seq-3) during the course of the experiment, suggesting that **1** was reacting preferentially with the Pu-GATG-Py-containing strand (Seq-2).

Furthermore, the overall rate of reaction was very slow with **1**/(Seq-2/Seq-3) intrastrand cross-link formation incomplete even after 24 h in contrast to reaction with Seq-1/Seq-1 which was complete after 3 h under the same conditions. Assignment of the 33.9 and 35.5 min peaks as monoalkylated and cross-linked single-stranded **1**/Seq-2 adducts, respectively, was confirmed by repeating the experiment with analogues of Seq-2 in which the guanine residues had been consecutively replaced with non-nucleophilic inosine bases. SJG-136 (**1**) was incubated separately with the annealed duplexes Seq-2A_{ino}/Seq-3 and Seq-2B_{ino}/Seq-3 (Table 1), which provided only single guanine binding sites (i.e., 5′-GATI-3′ and 5′-IATG-3′), thus allowing only monoalkylation. In both cases, peaks in the 33.9 min region (RT 33.4 and 33.7 min, Figure S5 and S7; Supporting Information) were obtained, identified as **1**/Seq-2A_{ino} and **1**/Seq-2B_{ino} adducts by MALDI-TOF MS. Therefore, the RT 33.9 min peak was assigned as the monoalkylated **1**/Seq-2 adduct, and the RT 35.5 min peak as the cross-linked **1**/Seq-2 single-stranded adduct by default. Direct reaction of **1** with single-stranded oligonucleotides Seq-2, Seq-2A_{ino}, and Seq-2B_{ino} was attempted as a control but failed in each case, thus confirming that duplex DNA is required for PBDs to react covalently with DNA. This suggested that the single-stranded adducts at RT 33.4 and 33.7 min must have arisen from denaturation of the equivalent duplex adducts, also explaining the excess of the nonguanine-containing Seq-3 (RT 27.3 min) in the HPLC traces.

Further observation showed that **1** initially formed the duplex intrastrand cross-linked adduct (RT 30.3 min; *m*/*z* 7842) from the Seq-2/Seq-3 duplex thus consuming both SS DNA species

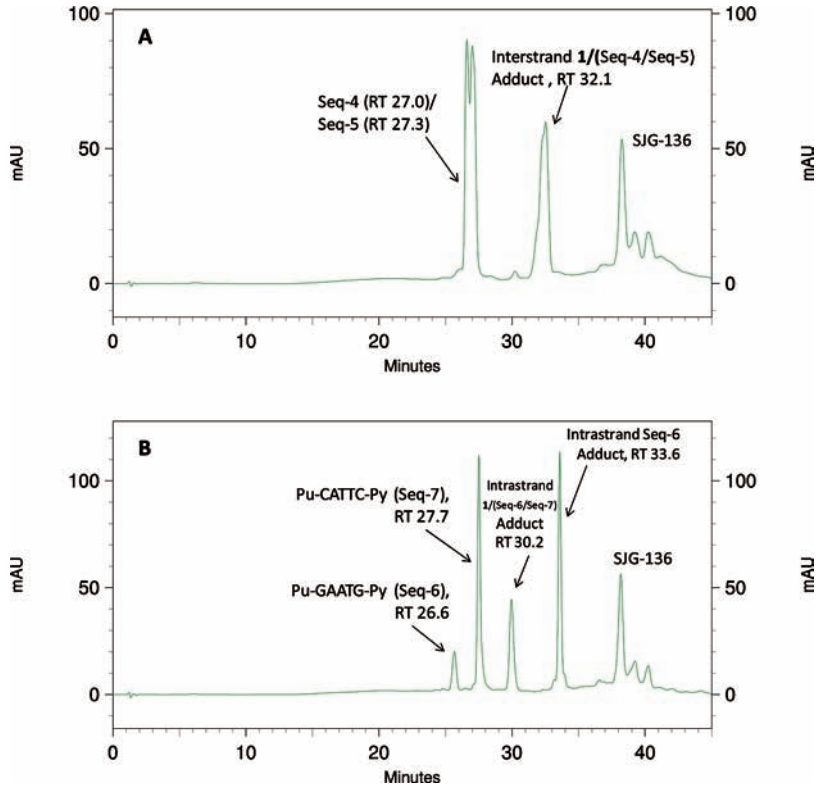

Figure 4. HPLC chromatograms: (A) Interstrand cross-linked adduct formed between **1** and the extended sequence Pu-GAATC-Py (Seq-4/Seq-5 duplex) after 5 min. (B) Intrastrand cross-linked adduct formed between **1** and the extended Pu-GAATG-Py sequence (Seq-6/Seq-7 duplex) after 5 min. Note the rapid reaction of **1** with the extended intrastrand cross-linking Pu-GAATG-Py sequence which minimizes production of slower-forming monoalkylated adducts.

at an equal rate (Figures S3C and S4A; Supporting Information). However, unlike the duplex interstrand cross-linked adduct which is stable to the HPLC conditions because of the covalent bonds linking both oligonucleotide strands,[19] a fraction of the intrastrand **1**/(Seq-2/Seq-3) adduct dissociates into the **1**/Seq-2 intrastrand adduct (35.5 min; *m*/*z* 4240) and the free Seq-3 strand (27.3 min), causing a relative increase in the 27.3 min (Seq-3) peak compared to the 26.4 min (Seq-2) peak. Similarly, the peak at 33.9 min assigned to the **1**/Seq-2 monoalkylated adduct through the inosine experiments presumably results from denaturation of a monoalkylated duplex intermediate formed on-route to the duplex intrastrand cross-linked adduct. Interestingly, a molecular dynamics study of a duplex adduct with only one of the PBD units of **1** covalently attached indicated a propensity for the nonattached PBD unit to rotate by 180° and to become embedded in the minor groove with the electrophilic C11-position pointing outward and so unable to undergo nucleophilic attack by the potentially cross-linking guanine (see Supporting Information).

Further evidence for monoalkylation, previously unobserved for PBD dimers, was obtained by challenging **1** with oligonucleotides containing sequences which were either too short (i.e., Pu-GC-Py and Pu-GG-Py duplexes, Seq-8/Seq-8 and Seq-9/Seq-10, Table 1) or too long (i.e., Pu-GAAAATG-Py duplex, Seq-11/Seq-12, Table 1) for cross-link formation. These duplexes offered guanine-containing binding sites where only one PBD unit of **1** could react covalently, with the other PBD binding site either too close, making it sterically impossible to react, or too far away so that the linker could not stretch far enough for cross-link formation (Figure S13 to S16, Supporting Information). In each case, monoalkylated adducts were formed (structures confirmed by MS), although reaction rate was much slower compared to sequences where cross-link formation was possible, with adduct formation incomplete even after 24 h (see Supporting Information).

Taken together, these results suggested that **1** is not as adduct-type or DNA-sequence selective as previously thought. Although previous modeling studies had suggested that Pu-GATC-Py was the preferred cross-linking site for SJG-136 and related analogues (of similar length),[10,23,29] and that an additional base pair between the covalently modified guanines would not be tolerated,[8] we investigated next the effect of including one additional AT base pair between reactive guanines for both the interstrand (Seq-4/Seq-5) and intrastrand (Seq-6/Seq-7) cross-linking sequences. After incubation of **1** with the annealed Seq-4/Seq-5 duplex (Duplex-3) containing the extended Pu-GAATC-Py interstrand cross-linking site, gradual emergence of a new peak at 32.1 min was observed (Figure 4A), identified by retention time and MS as the **1**/(Seq-4/Seq-5) interstrand cross-linked adduct. The reaction was slower than for the standard Seq-1/Seq-1 duplex (with adduct formation still not complete after 24 h), suggesting that this sequence is less preferred than Pu-GATC-Py. Surprisingly, when **1** was incubated with the annealed Seq-6/Seq-7 duplex (Duplex-4) containing the extended intrastrand Pu-GAATG-Py binding site, two new peaks rapidly emerged at 30.2 and 33.6 min (Figure 4B), identified by retention time and MS as the **1**/(Seq-6/Seq-7) intrastrand cross-linked duplex adduct and the **1**/Seq-6 cross-linked single-stranded adduct, respectively, a result similar to the reaction of **1** with Seq-2/Seq-3 (Duplex-2) although significantly faster. In

(29) Bose, D. S.; Thompson, A. S.; Smellie, M.; Berardini, M. D.; Hartley, J. A.; Jenkins, T. C.; Neidle, S.; Thurston, D. E. *Chem. Commun.* **1992**, 1518–1520.

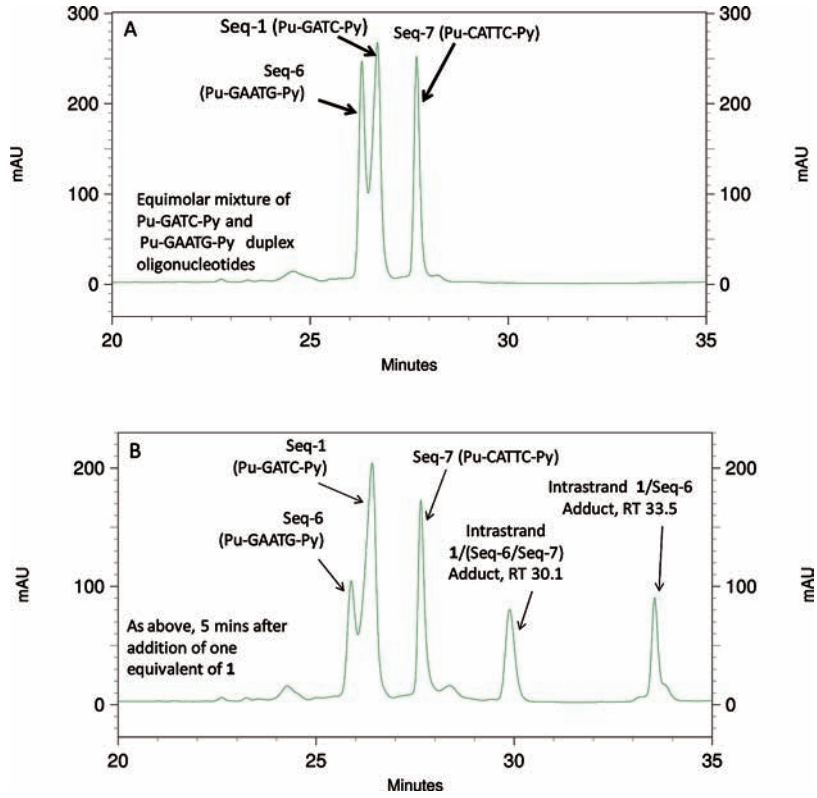

Figure 5. Competition experiment between Pu-GATC-Py (Seq-1/Seq-1) and Pu-GAATG-Py (Seq-6/Seq-7) using 1 equiv of SJG-136 (**1**). (A) HPLC analysis of an equimolar mixture of Pu-GATC-Py (Seq-1/Seq-1) and Pu-GAATG-Py (Seq-6/Seq-7) oligonucleotide duplexes. (B) 5 min after addition of 1 equiv of SJG-136 (**1**) to the mixture of duplex oligonucleotides (as in A above) at room temperature.

the chromatogram shown in Figure 4B measured after only 5 min incubation, denatured Seq-7 at 27.7 min remains a significant peak, and the intrastrand **1**/Seq-6 cross-linked adduct at RT 33.6 min is more prominent than the duplex **1**/(Seq-6/Seq-7) intrastrand cross-linked adduct at RT 30.2 min. This behavior contrasts with the results for the Pu-GATG-Py (Seq-2/Seq-3) sequence where the duplex **1**/(Seq-2/Seq-3) intrastrand cross-linked adduct was the major component (see Supporting Information). This might be accounted for by some distortion of the duplex adduct in the case of the extended Pu-GAATG-Py sequence leading to destabilization and greater dissociation of the adduct under the HPLC conditions with a shift of the equilibrium toward the intrastrand **1**/Seq-6 species. The rapidity of the reaction of **1** with the Seq-6/Seq-7 duplex (i.e., ~95% complete after 1 h) appeared to exclude the formation of monoalkylated adducts which were previously shown to form only slowly. Again, this result contrasted with the behavior of the Pu-GATG-Py (Seq-2/Seq-3) sequence which reacted slowly enough to allow the formation of monoalkylated adducts (Figure 3B). Control experiments were conducted using single-stranded Seq-2 (Pu-GATG-Py) and Seq-6 (Pu-GAATG-Py) oligonucleotides which both failed to react with **1** (as judged by independent HPLC and MALDI-TOF MS experiments) after incubation for 24 h, again demonstrating the requirement for minor-groove structure for PBD interaction and covalent bonding consistent with literature reports. These control experiments also ruled out the possibility of hairpin formation by these two single-stranded DNA sequences.

Next, a direct competition experiment was carried out between the interstrand cross-linking Pu-GATC-Py (Seq-1/Seq-1; Duplex-1) and intrastrand cross-linking Pu-GAATG-Py (Seq-6/Seq-7; Duplex 4)) duplexes in which 1 equiv of **1** was added to an equimolar mixture of annealed Seq-1/Seq-1 and Seq-6/Seq-7 at room temperature (Figure 5A). Immediate HPLC analysis (~5 min) showed the rapid emergence of peaks corresponding to the double-stranded intrastrand **1**/(Seq-6/Seq-7) (RT 30.1 min) and single-stranded intrastrand **1**/Seq-6 (RT 33.5 min) adducts, with no measurable amount of double-stranded interstrand **1**/(Seq-1/Seq-1) adduct (Figure 5B). Separate time-course studies with individual duplexes showed that at 0 h (~5 min), 82.2% of the intrastrand Seq-6/Seq-7 (Pu-GAATG-Py) adduct had formed compared to only 35.0% of the interstrand Seq-1/Seq-1 (Pu-GATC-Py) adduct (see Supporting Information). Furthermore, reaction with Seq-6/Seq-7 was nearly complete (~ 95.0%) after 1 h, whereas 3 h were required for completion of reaction with Seq-1/Seq-1. These results demonstrated unequivocally that **1** prefers intrastrand cross-linking with Pu-GAATG-Py compared to interstrand cross-linking with Pu-GATC-Py by a factor of at least 2.5 times. Further similar experiments allowed comparison of reaction rates with the intrastrand Seq-2/Seq-3 (Pu-GATG-Py) and interstrand Seq-4/Seq-5 (Pu-GAATC-Py) oligonucleotide duplexes. Both were relatively slow and did not complete reaction with **1** even after 24 h. The comparative data shown in Figure 6 provide a clear rank order of reactivity of Pu-GAATG-Py > Pu-GATC-Py ≫ Pu-GATG-Py and Pu-GAATC-Py.

Molecular models were constructed to gain insight into the structures of the previously unobserved intrastrand cross-linked adducts of **1** with the Pu-GATG-Py (Seq-2/Seq-3; Duplex-2) and Pu-GAATG-Py (Seq-6/Seq-7; Duplex-4) sequences, the extended interstrand Pu-GAATC-Py (Seq-4/Seq-5; Duplex 3) adduct, and also the monoalkylated adduct formed with Pu-GATG-Py (Seq-2/Seq-3). From minimized models constructed with the AMBER(v9) software, **1** appears to be easily accom-

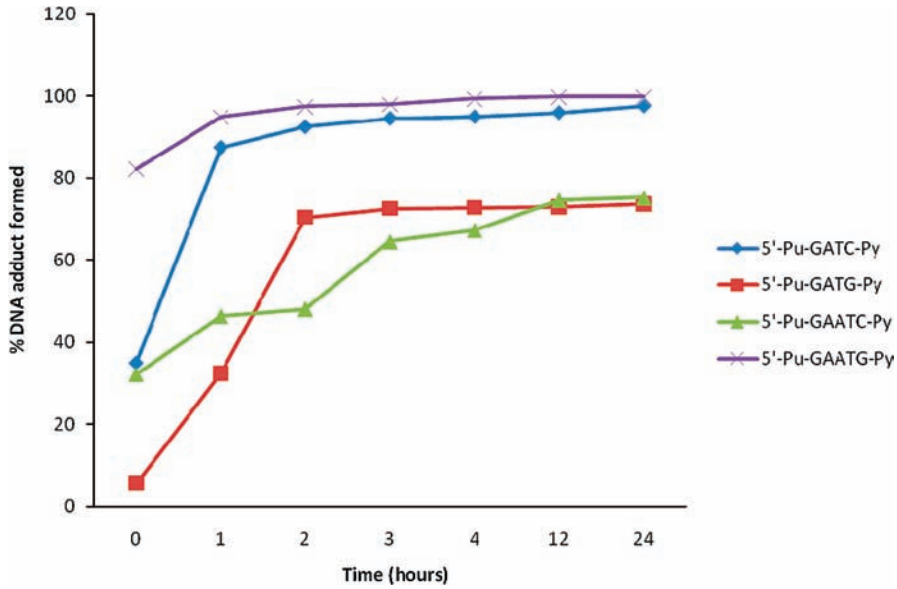

Figure 6. Comparison of reaction rates of SJG-136 (**1**) with annealed Seq-1/Seq-1 (Pu-GATC-Py), Seq-2/Seq-3 (Pu-GATG-Py), Seq-4/Seq-5 (Pu-GAATC-Py) and Seq-6/Seq-7 (Pu-GAATG-Py) oligonucleotide duplexes. Reactions were monitored by HPLC in separate experiments for 4:1 mol equiv mixtures of **1** and the individual duplex oligonucleotides, respectively. Adduct peaks were quantified against external standards (see Supporting Information).

modated by the participating guanines in the Pu-GATC-Py (Seq-1/Seq-1; Duplex-1) and Pu-GATG-Py (Seq-2/Seq-3; Duplex-2) sequences. However, in the extended sequences Pu-GAATC-Py (Seq-4/Seq-5; Duplex-3) and Pu-GAATG-Py (Seq-6/Seq-7; Duplex-4), **1** appears to be accommodated only at the expense of some distortion of the DNA at the points of covalent attachment, with **1** adopting a slightly lower position in the minor groove in order to span the distance between the reactive C2-NH_2 positions of guanines (i.e., 14.25 Å in Pu-GAATG-Py compared to 13.34 Å for Pu-GATG-Py according to the models). The total energies of energy-minimized adducts of identical DNA base-pair length and compositions were also compared. The interstrand **1**/(Seq-1/Seq-1) Pu-GATC-Py adduct had a slightly lower energy (−4326.2 kJ) compared to its isomeric intrastrand **1**/(Seq-2/Seq-3) Pu-GATG-Py adduct (−4322.2 KJ). Conversely, for the isomeric extended binding sites, the total energy was lower for the intrastrand **1**/(Seq-6/Seq-7) Pu-GAATG-Py (−4671.5 KJ) compared to the interstrand **1**/(Seq-4/Seq-5) Pu-GAATC-Py adduct (−4662.7 KJ) (see Supporting Information). Although these energy differences are small and may not be significant, they appear to reflect the possibility that, for the pairs of oligonucleotide duplexes of identical length, the interstrand **1**/(Seq-1/Seq-1) Pu-GATC-Py and intrastrand **1**/(Seq-6/Seq-7) Pu-GAATG-Py adducts from each pair are the thermodynamically preferred products. These two adducts were also found to be the most kinetically preferred from within each pair according to the HPLC experiments (see Figure 6).

The models were then used to compare adducts resulting from the interstrand Pu-GATC-Py (Seq-1/Seq-1) and intrastrand Pu-GATG-Py (Seq-2/Seq-3) sequences. Interestingly, with one PBD unit of **1** covalently linked to guanine-5 of Seq-1 or Seq-2 within either duplex, the electrophilic C11 atom of the second PBD unit appeared well-positioned to react with the C2-NH_2 of the second reacting guanine whether on the same (i.e., guanine-8, Seq-1, Duplex-2) or opposite (i.e., guanine-5 opposite strand, Seq-1, Duplex-1) strand. Spatially overlaying the two models by aligning their backbones emphasized the close proximity of these second reacting guanine C2-NH_2 groups, implying that the free PBD unit should be able to react with either to form intra- or interstrand cross-links with equal facility (see Supporting Information), thus consistent with the experimental observation that both types of cross-links can form.

Next, molecular dynamics simulations were performed over 2 ns on the cross-linked adducts of **1** with the extended Pu-GAATC-Py (Seq-4/Seq-5; Duplex-3) and Pu-GAATG-Py (Seq-6/Seq-7; Duplex-4) duplexes. The strain observed in the initial models became more evident during the course of the dynamics simulations, manifesting as conformational changes necessary to accommodate it. The distortion was observed to be greater in the case of the interstrand cross-linked model (Pu-GAATC-Py; Seq-4/Seq-5). Figure 7 shows representative frames from the molecular dynamics simulations at 220 ps. While the distortions appear to be accommodated by more-global conformational changes with maintenance of base pairing in the case of the intrastrand cross-linked adduct (Pu-GAATG-Py; Duplex-4; Figure 7B), for the interstrand adduct (Pu-GAATC-Py; Duplex-3; Figure 7A) the relief of strain first manifested itself as a local distortion of the guanine-5 residue of Seq-5 (highlighted in magenta) which aligned along the axis of the helix causing the neighboring adenine-6 (highlighted in red) to flip outward from the helix. Over the time-course studied, the adenine-6 eventually recovered its base pairing, but there were subsequent further distortions including a loss of base pairing for guanine-5 and further mismatches downstream. The greater distortion observed in the Pu-GAATC-Py interstrand model over the course of the simulation is also evident from graphs of rms deviation of atom coordinates and the distance variation between the C11/C11′ atoms of **1** when bound to the respective guanines (see Figures S33 and S34, Supporting Information). Taken together, these results support the experimental observation that the intrastrand cross-linked adduct (Pu-GAATG-Py) is favored in comparison to the Pu-GAATC-Py interstrand adduct.

To gain insight into possible precovalent association complexes formed between **1** and the DNA duplexes prior to covalent attachment, molecular dynamics simulations were performed over 2 ns with **1** bound noncovalently into the relevant four duplexes (Duplex-1 to Duplex-4) which allowed the free energy of the complexes to be calculated (Table 2).

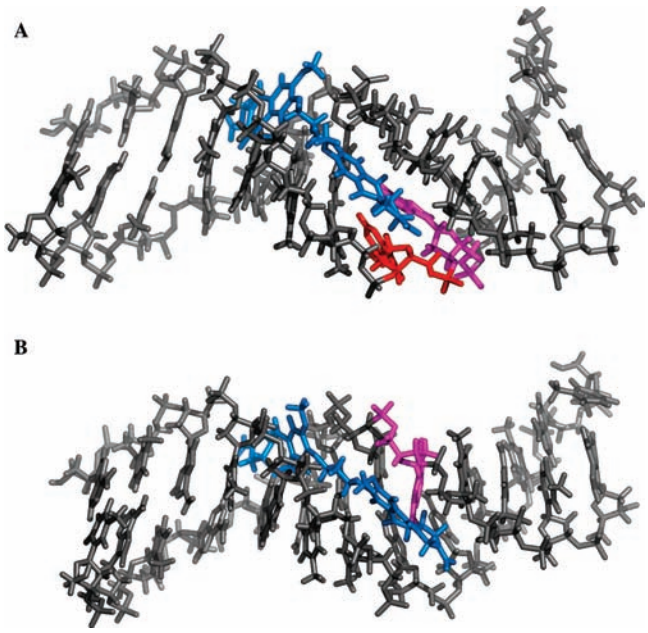

Figure 7. Representative frames from the molecular dynamics simulations (at 220 ps): (A) The **1**/(Seq-4/Seq-5) adduct containing the extended interstrand cross-linking Pu-GAATC-Py site. Note that residue G5 (magenta) of Seq-5 (Duplex-3) is distorted and has aligned along the axis of the helix causing the neighboring A6 (red) to flip outward from the helix. Over the time-course studied (2 ns), the A6 eventually recovered its base pairing, but there were subsequent further distortions including a loss of base pairing for G5 and further mismatches downstream. (B) The **1**/(Seq-6/Seq-7) adduct containing the extended intrastrand cross-linking Pu-GAATG-Py site. Note that G9 (magenta) of Seq-6 to which **1** is bound shows no major distortion. All atoms of **1** are blue, and the skeleton of the DNA duplex is gray.

Table 2. Calculated Changes in Free Energy (G) for Duplexes 1-4 After Non-Covalent Interaction With SJG-136 (**1**)

duplex sequences[a]	labels	ΔG^b
5′-TATAGATCTATA 3′-ATATCTAGATAT	Duplex-1	−54.58
5′-TATAGATGTATA 3′-ATATCTACATAT	Duplex-2	−53.34
5′-TATAGAATCTATA 3′-ATATCTTAGATAT	Duplex-3	−51.99
5′-TATAGAATGTATA 3′-ATATCTTACATAT	Duplex-4	−55.34

[a] Potential SJG-136 binding sites are underlined. [b] G = energy where ΔG = G(complex)-G(DNA)-G(ligand). Standard deviation values for ΔG values of Duplexes 1−4 were 3.14, 3.76, 3.23, and 4.12, respectively.

Again, although the differences in free energy are small and may be insignificant, the rank order of energies reflects the experimentally measured reaction rates for the four sequences as depicted in Figure 6. Interestingly, during the course of the dynamics simulations, a degree of migration of **1** along the minor groove was observed for Duplex-2 and Duplex-4 which have reacting guanines on the same stand, but occurred less significantly with Duplex-1 and Duplex-3 which have their guanines on opposite strands. For example, in one dynamics simulation with Duplex-4, the C11-position of one PBD unit of **1** was aligned with A6 of Seq-6 at the beginning of the simulation but moved to slightly downstream of G5 by the end of the run. In another simulation with Duplex-2, the C11-position of one PBD unit was initially aligned between G5 and A6 of Seq-2 but migrated to a position between A6 and T7 by the end of the run. These lateral movements of **1** in the minor groove could be due, in part, to local electrostatic repulsion between the partial negative charge on the N10/N10′-atoms of **1** (prior to covalent bond formation) and the negative partial charges present on the floor of the minor groove generated by the nitrogen atom of adenine and the oxygen atoms of thymine and cytosine bases. The effect with cytosine may be less pronounced since one N10-atom of **1** is oriented nearer to the strand to which the ligand covalently binds. Conversely, the partial positive charge on the C2-NH_2 hydrogens of guanine may provide an electrostatic attraction that pulls a N10 of **1** towards it, thus placing this C11-position in close proximity prior to covalent bond formation. It is noteworthy that, despite the repulsive effects, **1** showed no tendency to leave the minor groove during the simulation studies which may be due to the close-packing van der Waals attractions that exist. Monoalkylation adducts were also investigated, and the results further emphasized the tendency of **1** to become embedded in the minor groove. For example, initial models were constructed where only one PBD unit of **1** was covalently attached to a guanine, with the free PBD unit arranged to be pointing away from the minor groove. During dynamics simulation, the free PBD moved back into the minor groove with its C11-atom in a suitable position for the second alkylation event, whether inter- or intrastrand (Figures S28 and S29; Supporting Information). The distance between the C11/C11′-atoms of **1** was also observed to vary to a limited degree during the course of the dynamics simulation (Figure S30; Supporting Information).

Finally, the possibility that DNA "flexing" may contribute to the ability of **1** to effectively bridge between nucleophilic guanine C2-NH_2 groups was supported by similar modeling studies on monocovalent adducts. For example, one PBD unit of **1** was covalently bound to guanine-5 of the first strand (Seq-6) of Duplex-4, with the other PBD unit left unbound throughout the simulation. At the beginning of the simulation, the distance between the free C11-position of **1** and the N2 of G9 (Seq-6) was 7.94 Å. However, after 2 ns this distance had decreased to 3.11 Å (Figure S31A-C; Supporting Information) mainly due to flexing of the DNA but in part due to changes in the conformation of **1** as demonstrated by the variation in distance between the C11-atoms of its two PBD units (Figure S31C). In an identical experiment with the shorter Duplex-2, the equivalent distance did not shorten but instead fluctuated with a mean of 3.31 Å, so that the free C11-position of **1** remained in the vicinity of the N2 of G8 (Seq-2) throughout (Figure S32A-C; Supporting Information). These results suggest that covalent binding of **1** across two guanines separated by three base pairs rather than two (the more apparent natural fit) is accommodated mainly by changes to the DNA conformation but with some contributory stretching of the C8−O−$CH_2CH_2CH_2$−O−C8′ linkage that joins the two PBD units of **1**.

Taken together, these modeling results are consistent with the experimentally observed rates of reaction of **1** with Duplex-1 to Duplex-4. They are also consistent with an overall mechanism by which **1** enters the DNA minor groove followed by a degree of lateral movement to an energetically favored position prior to covalent bond formation. Next, one PBD unit presumably alkylates a guanine to form a monoalkylated adduct that will be the end product if no neighboring guanines are available. However, if a second guanine is available at an appropriate distance from the first, either on the same or opposite strand, then the other PBD unit will react to form an intra- or interstrand cross-link, respectively. Although the most appropriate distance between reacting guanines according to the models is when separation by two base pairs occurs (i.e., GATC or GATG), it

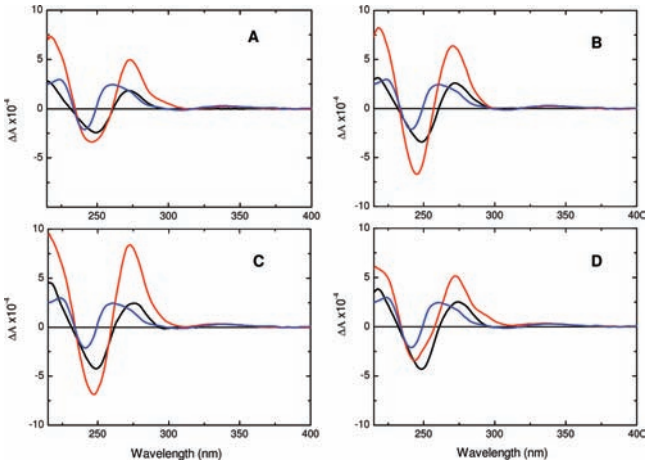

Figure 8. Far-UV circular dichroism (CD) measurements of DNA duplexes (1−4) before and after reaction with SJG-136 (**1**). (A) Interaction of **1** with Seq-1/Seq-1 duplex (Pu-GATC-Py). (B) Interaction of **1** with Seq-2/Seq-3 duplex (Pu-GATG-Py). (C) Interaction of **1** with Seq-4/Seq-5 duplex (Pu-GAATC-Py). (D) Interaction of **1** with Seq-6/Seq-7 duplex (Pu-GAATG-Py). Key: Duplex (black), SJG-136 (20 μM) (blue), Duplex/SJG-136 (1:4) (red).

would appear that when an extra base pair is inserted (i.e., GAATC or GAATG) the DNA can flex so that the guanines move toward each other and into appropriate positions for bis-covalent adduct formation with **1**.

A circular dichroism (CD) study was carried out to provide confirmation that a complex forms between **1** and the four oligonucleotide duplexes. Although CD measurements cannot distinguish between covalent and noncovalent bond formation, in this case the observed CD changes were assumed to represent covalent adduct formation, as this had been previously demonstrated for the same duplexes under identical conditions by HPLC/MS. The CD spectra of all duplexes changed significantly upon addition of **1** in the same ratio as used in the HPLC study, thus confirming that covalent adducts had formed (Figure 8). It has been previously reported that PBDs such as **1** do not react with non-hairpin-forming single-stranded oligonucleotides, and that no changes in CD signals are observed when PBDs are added to them.[30] Therefore, the enhancement of CD signals upon addition of **1** to the four oligonucleotides as shown in Figures 8A−D confirmed that these oligonucleotides were in duplex form prior to addition of **1**. However, the duplexes have low melting temperatures as the oligonucleotides are relatively short, therefore there is most likely an equilibrium between duplex and single-stranded forms. As the cross-linking agent **1** is added to each solution, the equilibrium should shift toward the duplex species, as the latter are stabilized by interstrand or intrastrand cross-links and potentially by monoalkylation adduct formation. In the presence of an excess of **1**, and given sufficient time, this process should drive cross-linked adduct formation to completion. The change in CD spectrum for the extended intrastrand Seq-6/Seq-7 duplex (Pu-GAATG-Py) as it reacts with **1** was also monitored at different temperatures. It is known from the literature that PBDs can detach from DNA at temperatures higher than 70 °C. As anticipated, a gradual loss of the **1**-induced CD signal was observed at temperatures higher than 67 °C, with complete loss of signal by 85 °C.

Finally, changes in UV absorption patterns over a range of temperatures were studied for the Seq-6/Seq-7 duplex (Pu-GAATG-Py) and its equivalent intrastrand cross-linked **1**/(Seq-6/Seq-7) adduct. A gradual increase in absorbance with temperature was observed at 260 nm for the Seq-6/Seq-7 duplex alone which started from 20 °C and continued until 37 °C at which point the strands had completely separated. However, for the **1**/(Seq-6/Seq-7) adduct, no change in melting occurred until 52.5 °C because of the stabilizing effect of **1** (see Supporting Information). Comparative melting studies were carried out on all duplexes, and the results are shown in Table 3 and Figure 9. The T_m values of the adducts (53−66 °C) were consistently higher than for the four duplexes alone (19−22 °C), thus confirming that stabilization through ligand binding was occurring in each case. As anticipated, the two interstrand cross-linked adducts **1**/(Seq-1/Seq-1) (Pu-GATC-Py) and **1**/(Seq-4/Seq-5) (Pu-GAATC-Py) had higher ΔT_m values (47 and 35 °C, respectively) compared to the equivalent intrastrand adducts **1**/(Seq-2/Seq-3) (Pu-GATG-Py) and **1**/(Seq-6/Seq-7) (Pu-GAATG-Py) (44 and 33 °C, respectively), reflecting the covalent binding of both strands of the Seq-1/Seq-1 and Seq-4/Seq-5 duplexes. It is noteworthy that the greatest DNA stabilization (47 °C) was observed for the interstrand **1**/(Seq-1/Seq-1) cross-linked adduct (Pu-GATC-Py) which is reported[19,20,22] to be the preferred cross-linking sequence for SJG-136 (**1**). The ΔT_m value for the extended interstrand **1**/(Seq-4/Seq-5) cross-linked adduct (Pu-GAATC-Py) was significantly lower (35 °C), consistent with the slight distortion of this cross-link (compared to the Pu-GATC-Py cross-link) observed in the molecular modeling studies. Similarly, the extended intrastrand Pu-GAATG-Py cross-linked adduct had a lower ΔT_m value (33 °C) compared to the shorter Pu-GATG-Py adduct (44 °C), again reflecting the slight distortion observed in modeling studies. Results for all the temperature/time-course experiment are shown in Figure 9 along with associated cooling data. The noncoincidence of the heating and cooling curves for all the adducts is a significant feature of the data set, most likely reflecting covalent disconnection of **1** from the DNA duplexes at higher temperatures with an inability to react again within the time frame of the experiment.

Conclusion

The observations reported here demonstrate that, in addition to the previously known interstrand cross-link at Pu-GATC-Py sequences, SJG-136 (**1**) can form a longer interstrand cross-link at Pu-GAATC-Py sequences, intrastrand cross-links at shorter Pu-GATG-Py and longer Pu-GAATG-Py sequences, and, in addition, monoalkylated adducts at suitable PBD binding sites where neither intra- nor interstrand cross-links are feasible due to the unavailability of a suitable second guanine. Interestingly, there is a preference for formation of the extended intrastrand cross-link with Pu-GAATG-Py which forms more rapidly than

Table 3. Melting Temperatures of DNA Duplexes and Their Respective Interstrand and Intrastrand Cross-Linked Adducts with **1**

DNA duplexes	melting temperatures of DNA duplexes alone (T_m, °C)	melting temperatures of cross-linked duplex adducts (T_m, °C)	ΔT_m (°C)
Seq-1/Seq-1(Pu-GATC-Py)	19	66 ± 0.89	47 ± 0.89
Seq-2/Seq-3(Pu-GATG-Py)	20	64 ± 0.21	44 ± 0.21
Seq-4/Seq-5(Pu-GAATC-Py)	22	57 ± 0.63	35 ± 0.63
Seq-6/Seq-7(Pu-GAATG-Py)	20	53 ± 0.35	33 ± 0.35

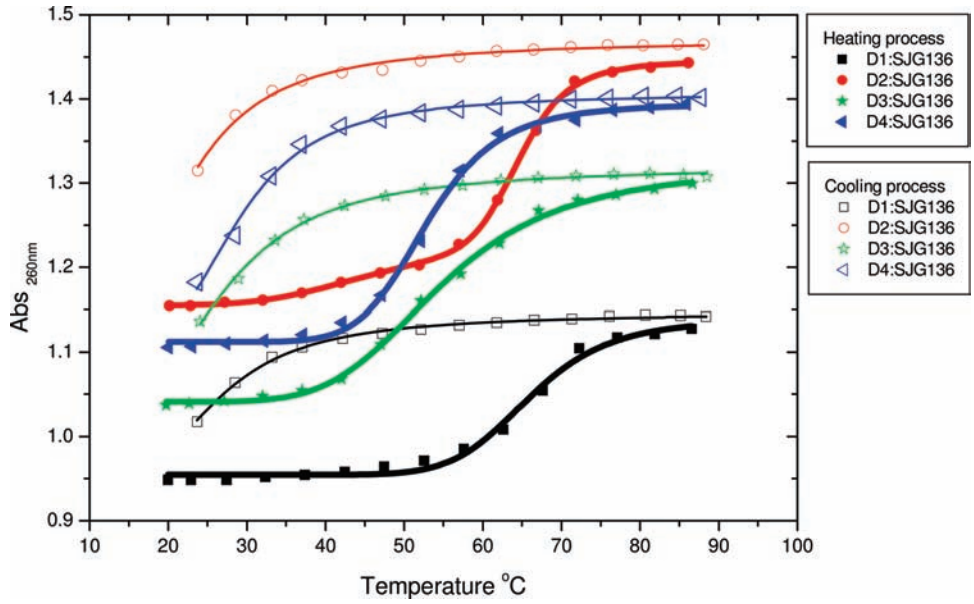

Figure 9. UV melting profiles of DNA duplexes and their cross-linked adducts at 260 nm. Key: D1 = **1**/(Seq-1/Seq-1) duplex adduct (Pu-GATC-Py), D2 = **1**/(Seq-2/Seq-3) duplex adduct (Pu-GATG-Py), D3 = **1**/(Seq-4/Seq-5) duplex adduct (Pu-GAATC-Py), D4 = **1**/(Seq-6/Seq-7) duplex adduct (Pu-GAATG-Py).

the other cross-link types (rank order: Pu-GAATG-Py > Pu-GATC-Py ≫ Pu-GATG-Py and Pu-GAATC-Py). However, thermal denaturation studies suggest that the originally reported Pu-GATC-Py interstrand cross-link is more stable, consistent with covalent bonding of both strands of the duplex and a lower overall distortion of the adduct according to modeling studies.

These results may explain previously reported DNA footprinting and in vitro transcription stop assay data for **1** which could not be completely explained on the basis of the interstrand Pu-GATC-Py cross-link alone.[20] For example, using a 260-base pair fragment of MS2 T7 DNA, a significant footprint and corresponding in vitro transcription stop site were observed at an occurrence of 5′-TCTATCC-3′ (3′-AGATAGG-5′) which could be due to an extended intrastrand cross-link (3′-GATAG-5′). Other sequences such as 5′-TGCGGATCCTC-3′ which also gave correlative footprints and in vitro stop assay sites contain both normal (5′-TGCGGATCCTC-3′) and extended (5′-TGCGGATCCTC-3′) interstrand cross-link sites (reactive GC base pairs underlined).

Taken together, these results indicate that SJG-136 (**1**) forms a wider variety of covalent DNA adducts than originally thought. This may have implications for the mechanism of action of this agent and the cellular mechanisms by which its DNA adducts are repaired. The latter could impact on the manner by which tumor cells develop resistance to SJG-136 and suggest the need for additional types of assays to measure the PD end point in clinical trials. For example, the COMET assay[31] used to date is optimized to detect interstrand cross-links.

Materials and Methods

Single-Stranded Oligonucleotides (Seq-1 to Seq-12). Single-stranded (SS) oligonucleotides were obtained in lyophilized form from AtdBio Ltd (UK). They were annealed to form duplex (DS) DNA according to the procedure below.

Double-Stranded Oligonucleotides. Each oligonucleotide was dissolved in 100 mM ammonium acetate (Sigma-Aldrich UK) to form a stock solution of 2 mM which was later diluted to 1 mM by addition of annealing buffer (10 mM Tris/50 mM sodium chloride/1 mM EDTA). Solutions of double-stranded DNAs were prepared by heating the complementary SS sequences (1 mM) in annealing buffer (pH 8.5) to 70 °C for 10 min in a heating/cooling block (Grant Bio UK). The solutions were then allowed to cool slowly to room temperature followed by storage at −20 °C overnight to ensure completion of the annealing process. Working solutions of DNA duplexes of 50 μM were prepared by diluting the stored stock solutions with 20 mM ammonium acetate.

PBD Dimer 1 (SJG-136). SJG-136 was supplied by Spirogen Ltd (Batch No: SG2000.003) and was dissolved in 50/50 v/v methanol/water to form a stock solution of 3 mM which was stored at −20 °C for no longer than four months. Working solutions of the drug of 200 μM were prepared by diluting the stock solution with nuclease free water. These were stored at −20 °C for not more than one week and thawed to room temperature for use when required.

Preparation of Adducts of 1 and DNA. Ligand/DNA adducts were prepared by incubating **1** with single-stranded or duplex oligonucleotides at a 4:1 molar ratio at room temperature. Samples were withdrawn at various time intervals and subjected to ion-pair RPLC and MALDI-TOF mass spectrometry analysis as described below.

Ion-Pair Reversed-Phase Liquid Chromatography (RPLC) Analysis. Liquid chromatography was performed on a Thermo Electron HPLC system equipped with a 4.6 × 50 mm Xterra MS C18 column packed with 2.5 μM particles (Waters Ltd, UK), an UV 1000 detector, an AS3000 autosampler, a SCM1000 vacuum degasser, and Chromquest software (Version 4.1). A gradient system of 100 mM triethyl ammonium bicarbonate (TEAB) as buffer A and 40% acetonitrile in water (HPLC grade, Fischer Scientific, UK) as buffer B was used. For buffer A, a 1 M preformulated buffer of TEAB was purchased from Sigma-Aldrich (UK) and diluted to 100 mM with HPLC grade water (Fischer Scientific, UK). The gradient was ramped from 90% A at 0 min to 70% A at 20 min, 60% at 25 min, and finally to 10% A at 40 min. UV absorbance was monitored at 254 nm, and fractions containing separated components were

(30) Rahman, K. M.; Mussa, V.; Narayanaswamy, M.; James, C. H.; Howard, P. W.; Thurston, D. E. *Chem. Commun.* **2009**, 227–229.
(31) Hartley, J. M.; Spanswick, V. J.; Gander, M.; Giacomini, G.; Whelan, J.; Souhami, R. L.; Hartley, J. A. *Ann. Oncol.* **1998**, *9*, 645.

collected manually, combined when appropriate, lyophilized, and analyzed using a MALDI TOF mass spectrometer as described below.

Mass Spectrometry Analysis (MALDI TOF). The covalently bound **1**/DNA adduct samples were prepared by diluting with matrix (1:1 mixture of 37 mg of THAP in 1 mL of ACN, and 45 mg of ammonium citrate in 1 mL of water) in ratios of 2:1, 1:1, or 1:5 (sample:matrix), and each examined for provision of best spectrum. One microliter of this mixture was then spotted onto the MALDI target plate and allowed to dry. Analysis was carried out on a Voyager DE-Pro with a nitrogen laser in positive linear mode using delayed extraction (500 ns) and an accelerating voltage of 25 000 V. Acquisition was between 4000−15 000 Da with 100 shots/spectrum.

General CD Studies. UV and CD spectra were acquired using a Chirascan spectrophotometer (Applied Photophysics, Leatherhead, UK). Suprasil 10 mm rectangular cells were employed for the wavelength region 400−215 nm. The instrument was flushed continuously with pure evaporated nitrogen throughout the experiment. The following parameters were employed: 1 nm spectral bandwidth, 1 nm step-size, and 1.5 s instrument time. All CD and UV spectra were buffer-baseline-corrected. The CD spectra were smoothed using the Savitsky−Golay method with a window factor of 4 and expressed in terms of ΔA.

Thermostability Studies. The UV and CD spectra of selected solutions were recorded initially at room temperature (20 °C) and then after heating to high temperature (90 °C), and again after recooling to 20 °C. The melting profiles were monitored at different wavelengths during both the heating and cooling phases. The instrument was equipped with a Quantum (North West) TC125 Peltier unit set to change temperature from 20→90 °C in 5 °C steps with 90 s temperature ramping and a 0.2 °C tolerance. A 0.2 s time-per-point CD measurement time and 1 nm step-size were employed for monitoring in the 400−215 nm region. Temperature was measured directly using a thermocouple probe in the sample solution, and melting data were fitted using a Levenberg−Marquart algorithm on the Van Hoff isochors.

Molecular Modeling. Molecular models were constructed in order to examine the structures of the DNA duplexes with and without ligand **1** bound. To test the integrity of the modeled structures under energetic conditions, dynamics simulations were carried out over 2 ns (nanoseconds) at room temperature (300 K). For comparison, and as a measure of the affinity of **1** for the different sequences, dynamics was also performed for the same constructs consisting of Duplexes 1−4 interacting with SJG-136 noncovalently and the free energy of binding calculated using the AMBER MM_PBSA approach. In this method, internal energies and nonbonded interactions (long-range cut off) derived from molecular mechanics were combined with the generalized Born (GB) continuum solvent method. Structures for the free energy calculations consisted of 100 models derived from the molecular dynamics simulation taken at equal intervals.

Initial models of DNA constructs were made using the 'nucgen' build module of the AMBER(v9) modeling software,[32] and ligands were constructed by means of MacroModel (v6.5).[34] The minimized structures were exported in 'pdb' format and converted to the 'mol2' format with Gasteiger charges by means of the AMBER 'antechamber' routine before missing parameters were constructed with the 'parmchk' program. Covalent binding of **1** to the C2-NH_2 functional groups of guanine residues was performed graphically using AMBER 'Xleap' utilizing 'parm99' and the general Amber force field parameters (gaff). Care was taken to ensure that the (*S*)-configuration was maintained at the C11-position of the central PBD ring at the point of attachment to a guanine N2-position, consistent with literature reports.[8] In the case of the noncovalent studies, **1** was placed in the minor groove equidistant between the reacting guanine NH_2 groups. In all cases, constructs were exported for subsequent minimization during which the DNA alone was restrained with a high force constant, allowing the ligand to adjust to the DNA environment. Further minimization steps were performed while gradually reducing the restraints to zero. Molecular graphics images were produced using the UCSF Chimera package from the Resource for Biocomputing at the University of California, San Francisco (supported by NIH P41 RR-01081). Dynamics simulations using the AMBER 'Sander' program were then performed. In Sander, the generalized Born/surface area (GB/SA) implicit solvent model was used with monovalent electrostatic ion screening simulated with SALTCON set to 0.2 M. The dynamics integration time-step used was 0.002 ps while constraining all bonds to hydrogen atoms using the SHAKE algorithm.[34] A temperature of 300 K was maintained using the Langevin thermostat (NTT = 3, GAMMA_LN = 2.0), and a long-range nonbonded cutoff of 100 (Å) was used.

For each dynamics simulation, a rms fit of each saved conformation was performed against the first dynamics frame as a measure of conformational variation. In addition, the distance between the nucleophilic nitrogens of the reacting guanine C2-NH_2 groups and each of the respective C11 atoms of ligand **1** was monitored. As a measure of the ability of SJG-136 to 'stretch' during the dynamics process, the distance between the C11 atoms at each end of the molecule was also monitored.

Acknowledgment. Spirogen Ltd is thanked for supplying a sample of **1** (SJG-136; batch no. SG2000.003). Drs. Alex Drake and Tam T.T. Bui of Kings College London are thanked for assisting with the CD studies. The Commonwealth Commission is acknowledged for providing a studentship to K.M.R.

Supporting Information Available: HPLC, CD, UV and MS data, and molecular models of interstrand and intrastrand adducts. This material is available free of charge via the Internet at http://pubs.acs.org.

JA902986X

(32) Case, D. A.; Darden, T. A.; Cheatham, T. E., III; Simmerling, C. L.; Wang, J.; Duke, R. E.; Luo, R.; Merz, K. M.; Pearlman, D. A.; Crowley, M.; Walker, R. C.; Zhang, W. ; Wang, B.; Hayik, S.; Roitberg, A.; Seabra, G.; Wong, K. F.; Paesani, F.; Wu, X.; Brozell, S.; Tsui, V.; Gohlke, H.; Yang, L.; Tan, C.; Mongan, J.; Hornak, V.; Cui, G.; Beroza, P.; Mathews, D. H.; Schafmeister, C.; Ross, W. S.; University of California: San Francisco, 2006.

(33) Howard, A. E.; Cieplak, P.; Kollman, P. A. *J. Comput. Chem.* **1995**, *16*, 243–261.

(34) Duan, Y.; Kumar, S.; Rosenberg, J. M.; Kollman, P. A. *J. Comput. Chem.* **1995**, *16*, 1351–1356.